Extended analysis of the field-angle-dependent heat capacity of (TMTSF)2ClO4 toward identification of the superconducting gap structure

Shingo Yonezawa, Yoshiteru Maeno, Denis Jérome

Journal of Physics: Conference Series **449** (2013) 012032 doi:10.1088/1742-6596/449/1/012032

Extended analysis of the field-angle-dependent heat capacity of $(TMTSF)_2ClO_4$ toward identification of the superconducting gap structure

Shingo Yonezawa[1], Yoshiteru Maeno[1], and Denis Jérome[2]

[1] Department of Physics, Graduate School of Science, Kyoto University, Japan
[2] Laboratoire de Physique des Solides, Université Paris-Sud, Orsay, France

E-mail: yonezawa@scphys.kyoto-u.ac.jp

Abstract. In this paper, we present detailed analyses of the field-angle dependence of the heat capacity of the quasi-one-dimensional superconductor $(TMTSF)_2ClO_4$ with various models of superconducting gap structure. We clarify that the superconducting gap structure with line nodes at $k_y = \pm 0.25b^*$ is the only structure that is consistent with our experiment, irrespective of the value of the anion gap. The observed field-angle dependence of the heat capacity indicates that two of the four nodes mainly contribute to the quasiparticle excitation.

1. Introduction

In modern researches of superconductivity, investigation of unconventional superconductors, which have anisotropic gaps with sign reversals, is one of the most important subjects. The "Bechgaard salts", consisting of tetramethyl-tetraselena-fulvalene (TMTSF) molecules and anions, are the first organic superconductors reported in 1980 [1, 2] and are among the longest-studied unconventional superconductors. The TMTSF family is also unique because they have archetypal quasi-one-dimensional (Q1D) electronic bands [3, 4, 5, 6]. Interestingly, the superconducting (SC) phase is located next to the spin-density-wave (SDW) magnetic insulating phase in the pressure-temperature phase diagram. Thus, the possibility of spin-fluctuation-mediated superconductivity has been proposed. Indeed, the existence of spin-fluctuation in the vicinity of the SC state has been recently investigated [7, 8, 9, 10].

We recently performed field-angle-resolved calorimetry of the ambient-pressure SC member of the TMTSF family: $(TMTSF)_2ClO_4$ [11]. We observed a peculiar modulation in the in-plane field-angle ϕ dependence of the heat capacity C (see Figs. 2(a) and (b)) with clear kinks at $\phi = \pm 10^\circ$. This modulation is attributed to the quasiparticle excitation with wavenumber $\boldsymbol{k}$ near SC gap nodes/zeros [12, 13]. The position of the kinks gives us a crucial information on its SC gap structure: The SC gap nodes or zeros are located at $\boldsymbol{k}$-points where the Fermi velocity $\boldsymbol{v}_F(\boldsymbol{k})$ points $\pm 10^\circ$ away from the crystalline a axis. From this information, we proposed that the "d-wave-like" [14] gap structure with nodes at $k_y = \pm 0.25b^*$ (structure D in Fig. 1) is most consistent with the experiment. The identification of the gap structure should provide a solid bases to understand interesting SC phenomena in the TMTSF family, such as a possible Fulde-Ferrel-Larkin-Ovchinnikov (FFLO)-like state in high fields [15, 16, 17, 18, 19, 20, 21, 22].

In this paper, we present detailed analyses of the heat capacity data assuming various models of superconducting gap structures. We clarify that the superconducting gap structure with line nodes at

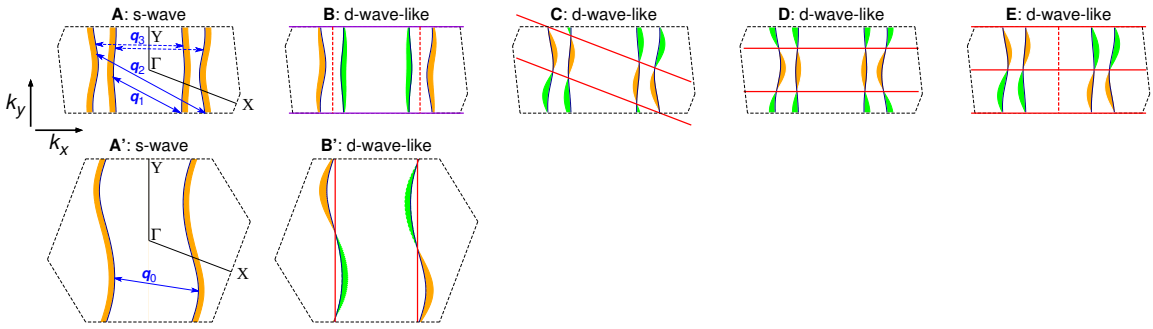

Figure 1. Schematic drawings of *s*-wave and *d*-wave-like superconducting gap structures. The orange and green colors indicate + and − signs of the superconducting gap, respectively. The red solid lines indicate nodal positions in the SC gap whereas the red broken lines indicate nodes that do not cut the Fermi surface. The purple lines in B indicate the positions of small gap minima. The first row exhibits gap structures for the split Fermi surface for $(TMTSF)_2ClO_4$. The structures in the second row are corresponding gap structures for the non-split Fermi surface for $(TMTSF)_2PF_6$. We here define k_x and k_y as a set of orthogonal basis in the reciprocal space as shown in the panel A. A and A′: *s*-wave state. The three nesting vectors [23] $\boldsymbol{q}_1$, $\boldsymbol{q}_2$, and $\boldsymbol{q}_3$ for the folded FS and the nesting vector $\boldsymbol{q}_0$ for the unfolded FS are also shown with blue arrows. Except the inter-band nesting vector $\boldsymbol{q}_3$, all the others are intra-band nesting vectors. B: *d*-wave-like state with small gap minima at $k_y = \pm 0.5b^*$ but without nodes. [24] B′: *d*-wave-like state, which turns into the structure B when the Fermi surface is folded due to the anion order. C: *d*-wave-like state with gap nodes running parallel to the Γ-X line. [25] D: *d*-wave-like state with gap nodes at $k_y = \pm 0.25b^*$. E: *d*-wave-like state with gap nodes at $k_y = 0$ and $\pm 0.5b^*$. For the structures C–E, no corresponding unfolded SC gap structures have been proposed.

$k_y = \pm 0.25b^*$ is the only structure that is consistent with our experiment, irrespective of the choice of the value of the anion gap Δ_{AO}, which causes the splitting of the quasi-one-dimensional Fermi surface into two pairs. The observed behavior indicates that two of the four nodes mainly determines the field-angle ϕ dependence of the heat capacity.

2. Possible Nodal Structures of the Superconducting Gap

Generally speaking, when the Fermi surface (FS) is strongly nested with a nesting vector $\boldsymbol{Q}_{\rm nest}$ and spin-singlet Cooper pairs are formed by the spin fluctuation with $\boldsymbol{Q}_{\rm nest}$, the SC gap $\Delta(\boldsymbol{k})$ and the pairing interaction $V(\boldsymbol{q})$ should satisfy the relation [4]

$$V(\boldsymbol{Q}_{\rm nest})\Delta(\boldsymbol{k})\Delta(\boldsymbol{k}+\boldsymbol{Q}_{\rm nest}) < 0 \quad (\boldsymbol{k}, \boldsymbol{k}+\boldsymbol{Q}_{\rm nest} \in \text{Fermi Surface}). \tag{1}$$

This is a direct consequence of the gap equation with assumption that $|V(\boldsymbol{q})|$ has a large peak at $\boldsymbol{q} = \boldsymbol{Q}_{\rm nest}$. For superconductivity near spin-density wave states, the value of $V(\boldsymbol{Q}_{\rm nest})$ should be positive. Thus, Eq. (1) can be simplified as

$$\Delta(\boldsymbol{k})\Delta(\boldsymbol{k}+\boldsymbol{Q}_{\rm nest}) < 0 \quad (\boldsymbol{k}, \boldsymbol{k}+\boldsymbol{Q}_{\rm nest} \in \text{Fermi Surface}). \tag{2}$$

The Brillouin zone (BZ) and FS of $(TMTSF)_2ClO_4$ is folded along the b^* direction due to the orientational order of the tetrahedral ClO_4 anions. Thus, the FS consists of two pairs of warped sheets as shown in Fig. 1(a). For this folded FS, three nesting vectors $\boldsymbol{q}_1$, $\boldsymbol{q}_2$, and $\boldsymbol{q}_3$ exists [23]; whereas for the unfolded FS shown in A′, $\boldsymbol{q}_0$ is the only nesting vector.

For $(TMTSF)_2ClO_4$, there are several candidates for its spin-singlet SC gap structure as shown in Fig. 1. For example, the *d*-wave-like structure B′ with line nodes, which has been theoretically predicted for the unfolded FS [26, 27, 28, 4], is folded resulting in the structure B [24]. The difference is that the nodes in B′ disappear and are replaced by small gap minima at $k_y = \pm 0.5b^*$ due to the split of the FS. Note that both structures B and B′ satisfy the relation (2) with $\boldsymbol{Q}_{\rm nest} = \boldsymbol{q}_3$ and $\boldsymbol{Q}_{\rm nest} = \boldsymbol{q}_0$, respectively. The structure C is recently predicted by Mizuno *et al* [25] for a certain situation where charge fluctuation contributes to the Cooper pairing [29]. This structure satisfies Eq. (2) with $\boldsymbol{Q}_{\rm nest} = \boldsymbol{q}_3$. We also list other possible structures D and E. For the structure D, Eq. (2) is satisfied with $\boldsymbol{Q}_{\rm nest} = \boldsymbol{q}_1$ and $\boldsymbol{q}_2$. Thus the intra-band nesting drives the pairing for this state. The structure E is similar to the structure C and the inter-band nesting $\boldsymbol{q}_3$ is important. We should note that the structures C, D, and E are essentially different from the structure B′, in the sense that b′ is not converted to C, D, and E by the FS folding.

For simplicity we only list *s*-wave and *d*-wave-like structures in Fig. 1. However, more complicated structure such as *g*-wave-like states [30] might also be possible. The present experiment is not phase-sensitive; thus we cannot distinguish structures with the same nodal positions but with different signs.

3. Anisotropy in the Doppler shift

Within the Doppler shift model, the heat capacity C of a Q1D superconductor with line nodes/zeros on its SC gap should depend on the field-direction ϕ with respect to the a axis as

$$C(\phi)/T \propto N(\phi) \propto (\Gamma^2 \sin^2\phi + \cos^2\phi)^{1/4} \sqrt{\frac{H}{H_{\rm c2}(0^\circ)}} \sum_{\rm n:nodes} A_{\rm n} |\sin(\phi - \phi_{\rm n})|, \tag{3}$$

as explained in Ref. [11]. Here, N is the quasiparticle density of states, $\phi_{\rm n}$ is the angle between the a axis and the Fermi velocity at a node, and $\Gamma \equiv H_{\rm c2}(\phi = 0^\circ)/H_{\rm c2}(\phi = 90^\circ)$ is the in-plane anisotropy ratio of the upper critical field $H_{\rm c2}$. The coefficient $A_{\rm n}$ represents the contribution of each node to the field-angle-dependent heat capacity. For superconductors with higher crystalline symmetry, all nodes should have the same value of $A_{\rm n}$. In contrast, because $(TMTSF)_2ClO_4$ has a triclinic crystal as well as band structures, the values of $A_{\rm n}$ may be different among different nodes; $A_{\rm n}$ should depend on the details of the band structure as well as of the SC gap structure near the gap node, e.g. the linear slope $\tilde{\Delta}$ of the gap around the node: $\Delta(\boldsymbol{k}) \sim \tilde{\Delta}|\boldsymbol{k} - \boldsymbol{k}_{\rm node}|$.

In Ref. [11], we chose $A_{\rm n2}/A_{\rm n1} = 0.3$ in order to demonstrate that the model captures important features of the experimental result, namely the asymmetry and the kink structures in the C/T vs. ϕ curve. However, as shown in Fig. 2, this choice of the value of $A_{\rm n2}/A_{\rm n1}$ is not very essential: as long as the condition $A_{\rm n2}/A_{\rm n1} \lesssim 0.7$ is satisfied, the observed behavior is reproduced.

The experimental result is hardly explained without the anisotropy in $A_{\rm n}$. This fact strongly suggest that the triclinic anisotropy in the band structure and the SC gap structure is important in the superconductivity of $(TMTSF)_2ClO_4$. Investigation of the origin of this anisotropy in $A_{\rm n}$, however, requires detailed theoretical calculations and is far beyond the scope of this paper.

We should note that recent theory [31] based on the Kramer-Pesch approximation also revealed that the observed behavior is indeed attributable to the existence of the gap node.

4. Anion-gap-energy dependence of the Fermi surface geometry

In the anion ordered state, there should be an anion gap energy $\Delta_{\rm AO}$, which corresponds to the difference in the on-site energy of the neighboring TMTSF chains driven by the anion order. In Ref. [11], we used the value $\Delta_{\rm AO} = 100$ meV deduced from the X-ray diffraction [23]. However, several transport studies have suggested smaller values of $\Delta_{\rm AO}$ such as 4.5 meV and 25 meV [32, 33]. In addition, a recent first-principle band calculation claimed that $\Delta_{\rm AO}$ is nearly zero [31]. Within the tight-binding model [23], when $\Delta_{\rm AO}$ becomes larger, the FS becomes flatter and the angle between the Fermi velocity and the a axis, $\phi_{\boldsymbol{v}_{\rm F}}$, tends to become smaller, as shown in Fig. 3.

This change in the Fermi surface geometry is important when we discuss the SC gap structure based on the experimental results.

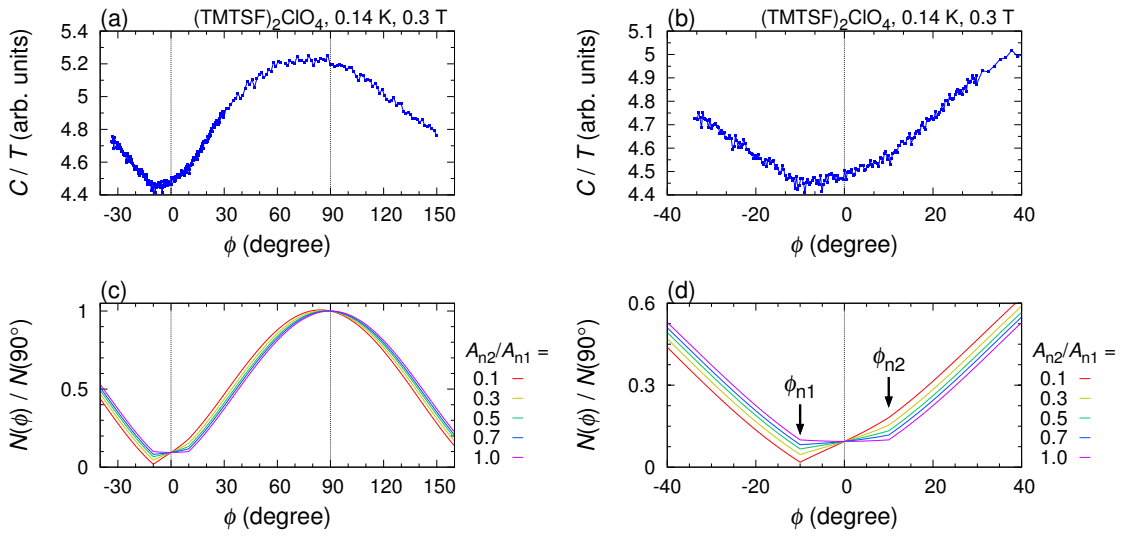

Figure 2. (a) In-plane field-angle ϕ dependence of the heat capacity of a $(TMTSF)_2ClO_4$ single crystal, measured at 0.14 K and 0.3 T [11]. The panel (b) is an enlarged view near $\phi = 0°$. (c) Normalized quasiparticle density of states (QDOS) $N(\phi)/N(90°)$ for $\Gamma = 3.5$, $(\phi_{n1}, \phi_{n2}) = (-10°, +10°)$, and $A_{n2}/A_{n1} = 0.1$, 0.3, 0.5, 0.7, and 1.0. The panel (d) is an enlarged view near $\phi = 0°$.

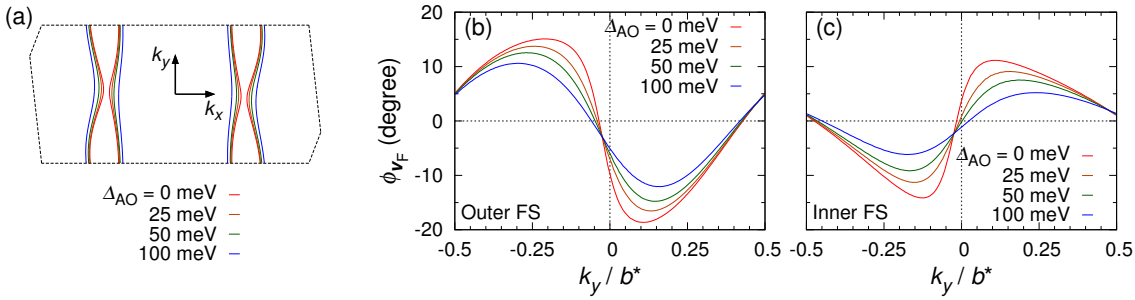

Figure 3. Dependence of the Fermi surface geometry on the anion gap energy Δ_{AO} calculated based on the tight-binding model. [23] (a) Fermi surfaces for different values of Δ_{AO}. (b) Anion-gap-energy dependence of $\phi_{\boldsymbol{v}_F} = \arctan(v_y/v_x)$ for the outer Fermi surface of the $k_x > 0$ side. (c) Anion-gap-energy dependence of $\phi_{\boldsymbol{v}_F}$ for the inner Fermi surface of the $k_x > 0$ side.

5. Detailed analysis of the gap structure

Here, we deduce the SC gap structure from the experimental results by comparing nodal structures shown in Fig. 1. It is also required to consider the dependence of the Fermi velocity on Δ_{AO} because there is some ambiguity in the value of Δ_{AO}. In Table 1, we list values of $\phi_{\boldsymbol{v}_F}^{node}$ for several superconducting gap structures and for different values of Δ_{AO}.

Our experimental results require that nodes of $\phi_{\boldsymbol{v}_F}^{node} \simeq +10°$ and of $\phi_{\boldsymbol{v}_F}^{node} \simeq -10°$ must *both* exist. In Table 1, if we allow error bars of 1°, there are only two possibilities that satisfy this condition: i.e. the structure D with $\Delta_{AO} = 0$ meV and with $\Delta_{AO} = 100$ meV; in case of $\Delta_{AO} = 0$ meV the inner FS has nodes of $\phi_{\boldsymbol{v}_F}^{node} \simeq \pm 10°$ whereas in case of $\Delta_{AO} = 100$ meV the outer FS has such nodes. Thus, irrespective of the value of Δ_{AO}, we can conclude that the structure with nodes at $k_y = \pm 0.25 b^*$ is the only possible nodal structure that is consistent with our experiment.

Table 1. Nodal direction in the velocity space (i.e. the angle between the Fermi velocity at the node and the a axis, $\phi_{v_F}^{node}$) for different gap structures and the anion gap energy. The values of $\phi_{v_F}^{node}$ for the outer FS (O-FS) and those for the inner FS (I-FS) are listed separately. Pairs of $\phi_{v_F}^{node}$ that are consistent with our experiment within an error bar of $\pm 1^\circ$ are shown with bold letters. The non-folded d-wave like structure B′ is also examined in the last column.

	$\phi_{v_F}^{node}$ for nodal structures listed in Fig. 1				
Δ_{AO} (meV)	structure B[†]	structure C	structure D	structure E	structure B′ [‡]
	O-FS / I-FS	O-FS / I-FS	O-FS / I-FS	O-FS / I-FS	
0	+5°, +1°	+5°, −12° / +9°, −13°	+15°, −14° / **+9°, −10°**	+5°, −10° / +1°, +2°	+11°, −18°
25	+5°, +1°	+5°, −9° / +5°, −11°	+13°, −13° / +8°, −9°	+5°, −8° / +1°, 0°	-
50	+5°, +1°	+5°, −7° / +3°, −9°	+12°, −12° / +7°, −7°	+5°, −7° / +1°, 0°	-
100	+5°, +1°	+5°, −6° / +1°, −6°	**+10°, −10°** / +5°, −5°	+5°, −5° / +1°, −1°	-

[†]For the structure B, which is a fully-gapped state, we list here ϕ_{v_F} at the gap minima at $k_y = \pm 0.5 b^*$.
[‡]Values for the non-folded structure B′ is calculated based on the high-pressure band structure in Ref. [23].

6. Contribution from all nodes

We for simplicity calculated $N(\phi)$ by taking into account of only the two nodes with $\phi_{v_F}^{node} = \pm 10^\circ$ in the preceding discussion. However, as shown in Fig. 1, the structure D has *four* nodes on its SC gap. Below, we will examine the contribution from the other two nodes.

In Fig. 4, we plot $N(\phi)/N(90^\circ)$ for the gap structure D with $\Delta_{AO} = 100$ meV (i.e. $(\phi_{n1}, \phi_{n2}, \phi_{n3}, \phi_{n4}) = (-10^\circ, +10^\circ, -5^\circ, +5^\circ)$) and $\Delta_{AO} = 0$ meV (i.e. $(\phi_{n1}, \phi_{n2}, \phi_{n3}, \phi_{n4}) = (-10^\circ, +9^\circ, -15^\circ, +14^\circ)$) with several sets of $(A_{n1}, A_{n2}, A_{n3}, A_{n4})$, the strength of nodal contribution to the heat-capacity oscillation. It is clear that the additional contributions of the nodes n3 and n4 do not alter the qualitative behavior of $N(\phi)$, unless A_{n3} and A_{n4} are as large as A_{n1}. Thus, the structure D is still consistent with the experiment. It is rather difficult to detect the contributions of all nodes even with the present high-resolution calorimeter, considering the signal-to-noise ratio of the data in Fig. 2(b).

7. Summary

In order to fully evaluate the superconducting gap structure from our calorimetry, we have examined several superconducting gap structures. We clarified that the superconducting gap structure with line nodes at $k_y = 0.25 b^*$ is the structure that is consistent with our field-angle ϕ dependence of the heat capacity C. The simplest example is shown in Fig. 1D, but possibility of a structure with the same nodal positions but with different signs (e.g. g-wave-like state) is not excluded. The conclusion on the nodal position is not altered irrespective of the value of the anion gap Δ_{AO}. We also demonstrate that the shape of the C/T-ϕ curve is mainly determined by nodes with large contributions to the heat capacity. This analysis guarantees the validity of the model in Ref. [11] taking into account of contributions from only two of the nodes.

Acknowledgments

We gratefully acknowledge H. Aizawa, Y. Suzumura, and A. Kobayashi for valuable discussion. This work is supported by a Grant-in-Aid for the Global COE "The Next Generation of Physics, Spun from Universality and Emergence" and by Grants-in-Aids for Scientific Research (KAKENHI 21110516, 21740253, 23540407, and 23110715) from MEXT and JSPS.

References

[1] Jérome D, Mazaud A, Ribault M and Bechgaard K 1980 *J. Phys. Lett.* **41** L95
[2] Bechgaard K, Carneiro K, Olsen M, Rasmussen F B and Jacobsen C S 1981 *Phys. Rev. Lett.* **46** 852
[3] Ishiguro T, Yamaji K and Saito G 1998 *Organic Superconductors Second Edition* (Heidelberg: Springer-Verlag)

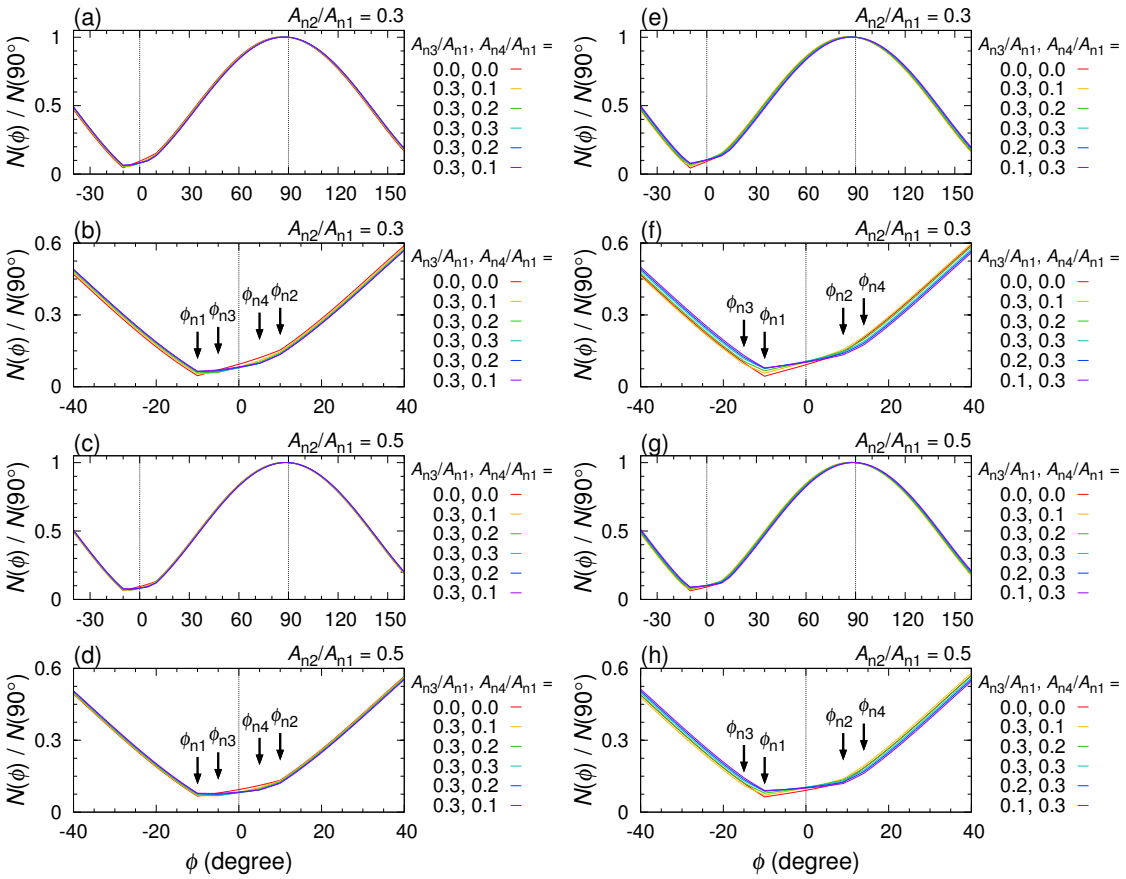

Figure 4. Normalized QDOS $N(\phi)/N(90°)$ for the gap structure D and for several sets of $(A_{n1}, A_{n2}, A_{n3}, A_{n4})$, the strength of nodal contribution to the heat-capacity oscillation. Here we used the in-plane anisotropy $\Gamma = 3.5$. (a)–(d) $N(\phi)/N(90°)$ for $(\phi_{n1}, \phi_{n2}, \phi_{n3}, \phi_{n4}) = (-10°, +10°, -5°, +5°)$. This set of $\{\phi_n\}$ corresponds to the anion gap $\Delta_{AO} = 100$ meV (See Table 1). (e)–(h) $N(\phi)/N(90°)$ for $(\phi_{n1}, \phi_{n2}, \phi_{n3}, \phi_{n4}) = (-10°, +9°, -15°, +14°)$. This set of $\{\phi_n\}$ corresponds to $\Delta_{AO} = 0$ meV.

[4] Kuroki K 2006 *J. Phys. Soc. Jpn.* **75** 051013
[5] Lee I J, Brown S E and Naughton M J 2006 *J. Phys. Soc. Jpn.* **75** 051011
[6] Jérome D 2012 *J. Supercond. Nov. Magn.* **25** 633
[7] Wu W, Chaikin P M, Kang W, Shinagawa J, Yu W and Brown S E 2005 *Phys. Rev. Lett.* **94** 097004
[8] Doiron-Leyraud N, Auban-Senzier P, de Cotret S R, Bourbonnais C, Jérome D, Bechgaard K and Taillefer L 2009 *Phys. Rev. B* **80** 214531
[9] Bourbonnais C and Sedeki A 2009 *Phys. Rev. B* **80** 085105
[10] Kimura Y, Misawa M and Kawamoto A 2011 *Phys. Rev. B* **84** 045123
[11] Yonezawa S, Maeno Y, Bechgaard K and Jérome D 2012 *Phys. Rev. B* **85** 140502(R)
[12] Volovik G E 1993 *JETP Lett.* **58** 469
[13] Vekhter I, Hirschfeld P J, Carbotte J P and Nicol E J 1999 *Phys. Rev. B* **59** R9023
[14] We note that the symmetries of these *d*-wave-like states are not lower than the crystalline symmetry. Thus, strictly speaking, they should not be called as the "*d*-wave" state in terms of the symmetry group theory. This is because we use the term "*d*-wave-like" here.
[15] Lebed A G 1986 *JETP Lett.* **44** 114
[16] Dupuis N and Montambaux G 1994 *Phys. Rev. B* **49** 8993
[17] Yonezawa S, Kusaba S, Maeno Y, Auban-Senzier P, Pasquier C, Bechgaard K and Jérome D 2008 *Phys. Rev. Lett.* **100** 117002
[18] Yonezawa S, Kusaba S, Maeno Y, Auban-Senzier P, Pasquier C and Jérome D 2008 *J. Phys. Soc. Jpn.* **77** 054712

[19] Aizawa H, Kuroki K, Yokoyama T and Tanaka Y 2009 *Phys. Rev. Lett.* **102** 016403
[20] Aizawa H, Kuroki K and Tanaka Y 2009 *J. Phys. Soc. Jpn.* **78** 124711
[21] Lebed A G 2011 *Phys. Rev. Lett.* **107** 087004
[22] Croitoru M D, Houzet M and Buzdin A I 2012 *Phys. Rev. Lett.* **108** 207005
[23] Pevelen D L, Gaultier J, Barrans Y, Chasseau D, Castet F and Ducasse L 2001 *Eur. Phys. J. B* **19** 363
[24] Shimahara H 2000 *Phys. Rev. B* **61** R14936
[25] Mizuno Y, Kobayashi A and Suzumura Y 2011 *Physica C* **471** 49
[26] Hasegawa Y and Fukuyama H 1987 *J. Phys. Soc. Jpn.* **56** 887
[27] Shimahara H 1989 *J. Phys. Soc. Jpn.* **58** 1735
[28] Duprat R and Bourbonnais C 2001 *Eur. Phys. J. B* **21** 219
[29] At first glance, the gap structure in Fig. 7 of Ref. [25] resembles the structure D. However, this is merely because an orthorhombic configuration is used for this figure; thus these nodes are actually parallel to the Γ-X line in the triclinic configuration (A. Kobayashi and Y. Suzumura, private communication.)
[30] Fuseya Y and Suzumura Y 2005 *J. Phys. Soc. Jpn.* **74** 1263
[31] Nagai Y, Nakamura H and Machida M 2011 *Phys. Rev. B* **83** 104523
[32] Uji S, Terashima T, Aoki H, Brooks J S, Tokumoto M, Takasaki S, Yamada J, and Anzai H 1996 *Phys. Rev. B* **53** 14399
[33] Yoshino H, Oda A, Sasaki T, Hanajiri T, Yamada J, Nakatsuji S, Anzai H and Murata K 1999 *J. Phys. Soc. Jpn.* **68** 3142